The ACCESS coupled model: documentation of core CMIP5 simulations and initial results

Martin Dix[1], Peter Vohralik[2], Daohua Bi[1], Harun Rashid[1], Simon Marsland[1], Siobhan O'Farrell[1], Petteri Uotila[1], Tony Hirst[1], Eva Kowalczyk[1], Arnold Sullivan[1], Hailin Yan[1], Charmaine Franklin[1], Zhian Sun[3], Ian Watterson[1], Mark Collier[1], Julie Noonan[1], Leon Rotstayn[1], Lauren Stevens[1], Peter Uhe[1] and Kamal Puri[3]

[1]Centre for Australian Weather and Climate Research (CAWCR), a partnership between CSIRO and the Bureau of Meteorology, CSIRO Marine and Atmospheric Research, Australia

[2]CSIRO Materials Science and Engineering, Australia

[3]CAWCR/Bureau of Meteorology, Australia

There are two versions of global coupled climate models developed at the Centre for Australian Weather and Climate Research (CAWCR) participating in phase 5 of the Coupled Model Inter-comparison Project (CMIP5), namely ACCESS1.0 and AC-CESS1.3. This paper describes the CMIP5 experimental configuration of the AC-CESS models and the climate forcings for the historical and future scenario runs.

We also present an initial analysis of model results, concentrating on changes in surface air temperature and the hydrologic cycle, and on climate sensitivity. Both models somewhat underestimate the observed 20th century warming, particularly in mid century, though recent warming rates match those observed. Mean warming for 2081–2100 relative to 1986–2005 under the RCP8.5 scenario is 3.61 K and 3.56 K for ACCESS1.0 and ACCESS1.3 respectively, and under RCP4.5 it is 2.34 K and 2.12 K.

Climate sensitivity from idealised simulations is 10–15 per cent larger in AC-CESS1.0 than ACCESS1.3 and both models are above the median of the range of CMIP3 and published CMIP5 results.

Introduction

Coupled climate models provide the basis for climate projection development and essential support for climate change attribution and for understanding climate change processes. In recognition of the need for a coordinated approach in the coupled modelling community to best support these areas of work, the World Climate Research Program's Working Group on Coupled Modelling has led development of an extensive set of coordinated experimentation for such models known as the Coupled Model Intercomparison Project phase 5 (CMIP5) (Taylor et al. 2012). The model simulations therein require adherence to a strict experimental protocol and also to a strict protocol for the format of the model output fields to facilitate ease of use by the climate analysis community (Taylor and Doutriaux 2010, Taylor et al. 2011). The distribution of these fields is to occur, in general, by the Earth System Grid (ESG), an

initiative led by PCMDI[1], which features a global distribution system involving interconnected nodes located in many nations engaged in climate system research (Williams et al. 2009). Analyses using the fields contributed to the ESG for CMIP5 will form the basis of the modelling contribution to the Fifth Assessment Report of the Intergovernmental Panel on Climate Change (IPCC AR5), due for publication during 2013 and 2014. However, CMIP5 is a long term project, and will continue well beyond the end of the IPCC AR5 process.

This paper documents the initial contribution of the Australian Community Climate and Earth System Simulator (ACCESS) to CMIP5. The ACCESS coupled climate model (hereafter ACCESS-CM) is documented in Bi et al. (2013). There are two versions of the ACCESS-CM, namely ACCESS1.0 and ACCESS1.3. These versions differ principally in the land surface component and in aspects of the atmospheric physics. In particular, ACCESS1.0 uses the MOSES2 land surface model (Essery et al. 2003) while

Corresponding author address: Martin Dix, email: martin.dix@csiro.au

ACCESS1.3 uses the CABLE land surface model (Kowalczyk et al. 2006, 2013). ACCESS1.0 uses the HadGEM2(r1.1) atmospheric physics (Martin et al. 2011, Collins et al. 2011) including the Smith (1990) cloud scheme, while ACCESS1.3 uses atmospheric physics similar to that of the Met Office GA1.0 model configuration (Hewitt et al. 2011), including the PC2 cloud scheme (Wilson et al. 2008). Both ACCESS1.0 and ACCESS1.3 are participating in CMIP5.

CMIP5 features three distinct experimental suites including: (1) decadal hindcast and prediction simulations; (2) simulations focussing on the longer term (up to multi-century timescales); and (3) 'time slice' simulations for atmosphere-only models that are particularly computationally challenging (Taylor et al. 2012). ACCESS1.0 and ACCESS1.3 are participating in the longer term experimental suite. This suite includes simulations for model evaluation, for projection and for improving understanding of climate change processes. The participation makes available ACCESS results for CMIP5 analysis studies, including those being performed in support of the IPCC AR5, and in further development of climate change projections. Participation in the decadal hindcast/prediction simulations is anticipated, but will await development of a suitable initialisation procedure. In each CMIP5 experimental suite, the priority for each simulation is designated 'core', 'tier 1' and 'tier 2', in order of decreasing priority. To date, only the 'core' simulations of the long-term suite have been performed with ACCESS1.0 and ACCESS1.3 and it is these simulations that are documented here. Selected 'tier 1' simulations are currently underway for both versions of the model and will be reported elsewhere. We anticipate that further 'tier 1' and 'tier 2' simulations will eventually be conducted, with selection depending on stakeholder interest and scientific importance.

This paper describes in detail the simulations conducted for ACCESS1.0 and 1.3, including details of the 'forcings' (solar, volcanic stratospheric aerosol, anthropogenic aerosol emissions and greenhouse gas concentrations) used. Key results from the historical and future scenario experiments are presented as well as the results of analyses from idealised experiments that explore model climate sensitivity.

CMIP5 experiment configuration and forcing

For the Fifth Assessment Report, the IPCC requested preparation of a new set of emission scenarios (Moss et al. 2010, van Vuuren et al. 2011). These were chosen to span the range of radiative forcing found in plausible published scenarios. There are four 'representative concentration pathways' (RCPs), named for the approximate radiative forcing in 2100. The RCPs include emissions of a wide range of well-mixed greenhouse gases (GHGs), aerosols and chemically active gases as well as land use changes.

The RCPs span a wider range than the SRES scenarios (Nakicenovic and Swart 2000) used in the modelling for both the IPCC Third Assessment (Cubasch et al. 2001) and the CMIP3 simulations (Meehl et al. 2005) which were used for the IPCC Fourth Assessment. In contrast to the SRES scenarios, some of the RCPs include the effects of mitigation policies.

Rogelj et al. (2012) used a reduced complexity model to simulate the response to all the RCP scenarios for a range of climate sensitivities and compared results to simulations using the SRES scenarios. They found that RCP8.5 was similar to the SRES A1FI scenario (warming more than the SRES A2 scenario which was commonly used as a high-end scenario in previous studies), RCP6 was similar to the SRES B2 scenario and RCP4.5 was similar to the SRES B1 scenario. RCP3 was lower than any of the standard SRES scenarios.

Of the RCPs, only RCP8.5 and RCP4.5 are CMIP5 core experiments and these are the only two future scenarios included in the ACCESS experiments described here. As well as these climate projection experiments, the CMIP5 core experiments performed with ACCESS include a preindustrial control experiment using 1850 forcing, an 1850–2005 historical experiment using observed changes in climate forcing agents, and idealised experiments using only CO_2 changes (one per cent/year compounding CO_2 growth and an abrupt four times CO_2 change).

In this section we describe aspects of the climate forcing in the CMIP5 simulations and in particular their implementation in the ACCESS models. Generally this is the same as the implementation in HadGEM2-ES, described in detail by Jones et al. (2011). However HadGEM2-ES includes interactive land and ocean carbon cycles and dynamic vegetation. These are not included in the ACCESS versions used here, nor do we include prescribed land use change. HadGEM2-ES also includes an interactive tropospheric chemistry scheme which, for example, simulates concentrations of ozone and other gas-phase species which interact with the aerosol scheme. By contrast, in ACCESS, concentrations of the gas-phase species which are used in the sulphur oxidation scheme are prescribed.

Other aspects in which ACCESS differs from HadGEM2-ES will be highlighted in discussion of particular forcings. Unless mentioned otherwise the implementation in ACCESS1.0 and ACCESS1.3 should be considered identical. Both models have an atmospheric resolution of 1.875° by 1.25° in the horizontal with 38 vertical levels and an atmospheric top at approximately 40 km. The ocean model has 50 vertical levels and 1° horizontal resolution, increasing to 1/3° near the equator (Bi et al. 2013).

We discuss aerosols in particular detail because in this case only precursor emissions are prescribed rather than concentrations and so one might expect concentrations (and so radiative forcing) to be more model dependent than is the case for other forcing agents.

Well-mixed greenhouse gases

For use in CMIP5, the MAGICC model was used to derive a consistent set of GHG concentrations from the RCP emissions (Meinshausen et al. 2011a). Figure 1 shows the CO_2

concentrations for the four scenarios and Fig. 2 shows the evolution of the total GHG radiative forcing from MAGICC relative to 1850—the start date of the ACCESS historical experiment.

The model radiation scheme explicitly treats CO_2, CH_4, N_2O and the halocarbons CFC11, CFC12, CFC113, HCFC22, HCF125 and HFC134a. The RCPs include a much larger set of halocarbons and these were aggregated to equivalent CFC-12 and HFC134a concentrations (Jones et al. 2011). All these gases are prescribed as annual global mean concentrations with no horizontal or vertical variation. CO_2 is also passed to the model vegetation scheme where it affects plant stomatal resistance. The preindustrial control experiments used the 1850 values for all gases.

Ozone

Cionni et al. (2011) describe the preparation of the CMIP5 ozone dataset used here. The historical data was based on extending data from the well observed 1979–2009 period using correlations with stratospheric chlorine and the solar cycle. Future ozone projections are from the multi-model ensemble mean of a set of coupled chemistry climate models in order to include the effect of climate change. Note that these models all used the A1B greenhouse gas (GHG) scenario and the stratospheric ozone is the same in all RCP experiments. Springtime Antarctic ozone starts to decrease around 1960 with a steep decline in the mid 1970s. The minimum ozone occurs about 1995 but the recovery is slow and projected ozone only approaches the pre 1960s values by 2100.

For HadGEM2-ES and ACCESS, the stratospheric component of the standard future ozone scenario was modified to include solar cycle variability consistent with the prescribed future solar cycle (Jones et al. 2011). For tropospheric ozone, the ACCESS models also used the projections from Cionni et al. (2011), whereas in HadGEM2-ES tropospheric ozone was calculated via the coupled chemistry model. Although the standard CMIP5 dataset includes three-dimensional tropospheric ozone, the ACCESS model configuration uses zonal-mean values based on this dataset for both the troposphere and the stratosphere. This does not significantly affect the ozone radiative forcing.

Solar

The CMIP5 recommended data source for the total solar irradiance (TSI) is Lean (2009) which uses the methods of Fröhlich and Lean (2004) to calculate the solar cycle component and includes the longer term background variation from Wang et al. (2005). Annual means over the period of the experiments described here are shown in Fig. 3. The CMIP5 specification recommends scaling the TSI by a factor 0.9965 to match the recent Total Irradiance Monitor (TIM) data (Kopp and Lean 2011) which is a reduction of approximately 5 W m^{-2}. This correction was not used in the ACCESS simulations because it was too different from the value used in earlier developmental control simulations and

Fig. 1. Evolution of CO_2 concentration in the RCPs (Meinshausen et al. 2011a).
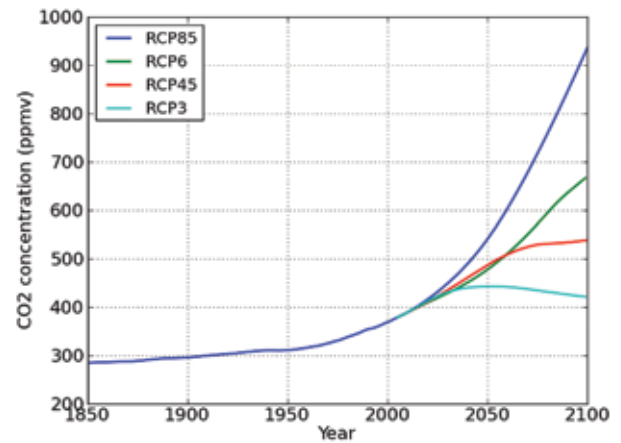

Fig. 2. Evolution of total greenhouse gas radiative forcing (relative to 1850) in the RCPs (calculated from Kyoto equivalent CO_2 in the RCP concentration data). These radiative forcings are derived using MAGICC (Meinshausen et al. 2011a) and the actual radiative forcings in the individual CMIP5 models may differ somewhat.
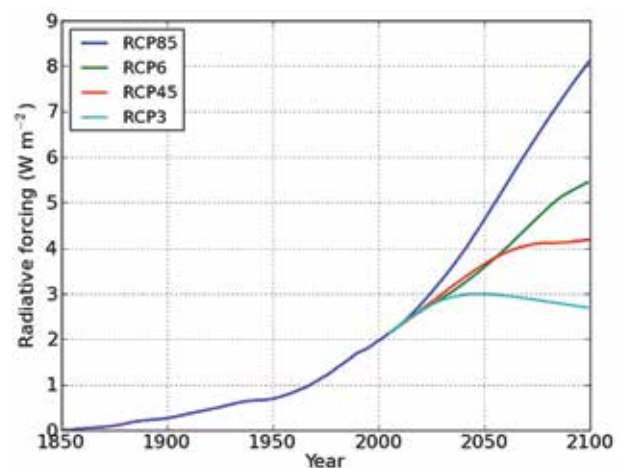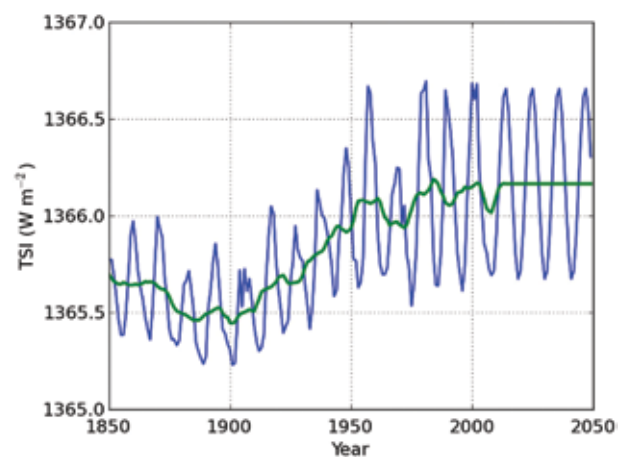

Fig. 3. Total solar irradiance from Lean (2009). The heavy green line is an 11-year running mean.

would have significantly affected the model global energy balance. Note however that this scaling has a negligible effect on the magnitude of the variations in the TSI and the changes in radiative forcing.

Jones et al (2011) show the time series of the solar irradiance variations in the spectral bands used in HadGEM2-ES (and also in the ACCESS models). The peak to peak variation in the UV (200–320 nm) is 0.5 per cent compared to only 0.07 per cent in the total.

The preindustrial control experiment used the 1844–1856 average values of solar irradiance.

Volcanic stratospheric aerosol

Stratospheric volcanic aerosol in the historical and RCP simulations is treated in the same way as in HadGEM2-ES (Jones et al. 2011). The CMIP5 specified data source is the monthly mean optical depth in four latitude bands from Sato et al. (1993), extended to the year 2000. Jones et al. (2011) describe the extension past 2000 with an eventual relaxation to the background value used in the pre-industrial control run by 2040.

The CMIP5 recommendation is that either volcanic aerosols should be omitted entirely from both the control and future runs, or, alternatively, the same background aerosol should be prescribed in both runs (Taylor et al. 2009). Here, for consistency with the RCPs, the control experiment should include a background stratospheric volcanic aerosol. However, the ACCESS experiments inadvertently did not include this in the preindustrial control runs. The time mean volcanic aerosol optical depth over 1850–2000 is 0.013 while HadGEM2-ES used a background value of 0.0097. Using this latter value with the forcing relation in Hansen et al. (2005) gives a approximate radiative forcing of –0.2 W m^{-2}. For comparison the net radiative forcing (GHG plus aerosol) in the year 2000 is approximately 2 W m^{-2} (Meinshausen et al. 2011a) and so the mean volcanic term is not negligible. As a consequence, the ACCESS historical and RCP simulations will be biased slightly cool relative to the preindustrial control, which will most affect fields sensitive to the time integrated warming such as sea level.

The MAGICC model has been widely used to calculate both GHG concentrations from emissions and also temperature change in response to GHG changes (Meinshausen et al. 2011b). It can also be used to estimate the effect of control experiment volcanic forcing by comparing runs with and without time mean volcanic forcing removed. For a first order estimate of the effect of the preindustrial volcanic forcing it is not necessary that MAGICC be tuned to closely reproduce the ACCESS simulations and we use the default configuration with a climate sensitivity of 3 K. These MAGICC simulations show that the surface warming in 2000 relative to 1850 (or relative to a preindustrial control) is reduced by 0.1 K. However, in practice, model warming is usually calculated with respect to an earlier part of an historical run with the control run only used to calculate climate drift. The effect of the time mean volcanic forcing equilibrates quite

quickly and year 2000 anomalies calculated relative to the 1850–1900 mean show almost no impact. The possible effect on ACCESS sea-level simulations is discussed by Marsland et al. (2013).

Tropospheric aerosols

The aerosol scheme used for both ACCESS1.0 and ACCESS1.3 is the Coupled Large-scale Aerosol Simulator for Studies In Climate (CLASSIC) (Bellouin et al. 2011). The scheme is used to simulate seven aerosol types with multiple components: sulphate aerosols (SO$_4$) (from DMS and SO$_2$ emissions and the sulphur cycle), fossil fuel black carbon (FFBC), fossil fuel organic carbon (FFOC), biomass-burning aerosols (BB) (with assumptions about the proportions of organic carbon and black carbon), secondary organic aerosols from vegetation terpene emissions (biogenic), sea salt (SS), and mineral dust (DU). Nitrate aerosols are not included in the ACCESS CMIP5 simulations.

Modelled aerosols exert direct radiative effects by scattering or absorbing short-wave and long-wave radiation. Apart from mineral dust and FFBC, which are assumed to be hydrophobic in the CLASSIC scheme, aerosols in the model also act as cloud-condensation nuclei and are able to affect the radiative balance through the first (cloud albedo) and second (cloud lifetime) indirect effects (Jones et al. 2001).

The magnitude of the aerosol direct effect is closely related to the wavelength-dependent aerosol optical depth (AOD), which gives the column-integrated aerosol extinction by scattering and absorption. AOD changes at 550 nm over the industrial period for the ACCESS1.0 historical simulation are illustrated by the green curves in Fig. 4. For aerosols which are predominantly natural in origin (SS, DU, biogenic), the optical depths remain relatively constant with time, although with large year-to-year variability in the case of dust. For aerosols with large anthropogenic sources (SO$_4$, FFOC, FFBC, BB) the modelled optical depths reflect increasing emissions over the historical period, followed by projected decreases over the 21st century for the RCP4.5 and RCP8.5 scenarios (blue and red curves). Further discussion of these results is given below.

Aerosols in the ACCESS models are prognostic except for sea salt and biogenic aerosols. Sea salt concentrations are diagnosed at each time step over the ocean based on near-surface wind speed (and are zero over land). Biogenic aerosols are prescribed by a monthly-varying mass mixing ratio (MMR) climatology. For more details about the CLASSIC scheme (including aerosol components used, particle size distributions and the interaction of aerosols with radiation) see Bellouin et al. (2007, 2011) and Jones et al. (2011).

The dust uplift scheme used in the ACCESS models is based on Woodward (2011) and is a revised version of the scheme discussed in Woodward (2001). The scheme models the horizontal flux of dust in nine size bins spanning particle diameters from 0.06 to 2000 μm, with dust uplift and transport occurring for the smallest six bins (particle diameters from 0.06 to 73.2 μm). Dust uplift can occur over

Fig. 4.   Time series of global annual mean aerosol optical depths at 550 nm in the ACCESS1.0 simulations. All values have been scaled by a factor 1000. Note that the y-axis scale and offset varies for each species.
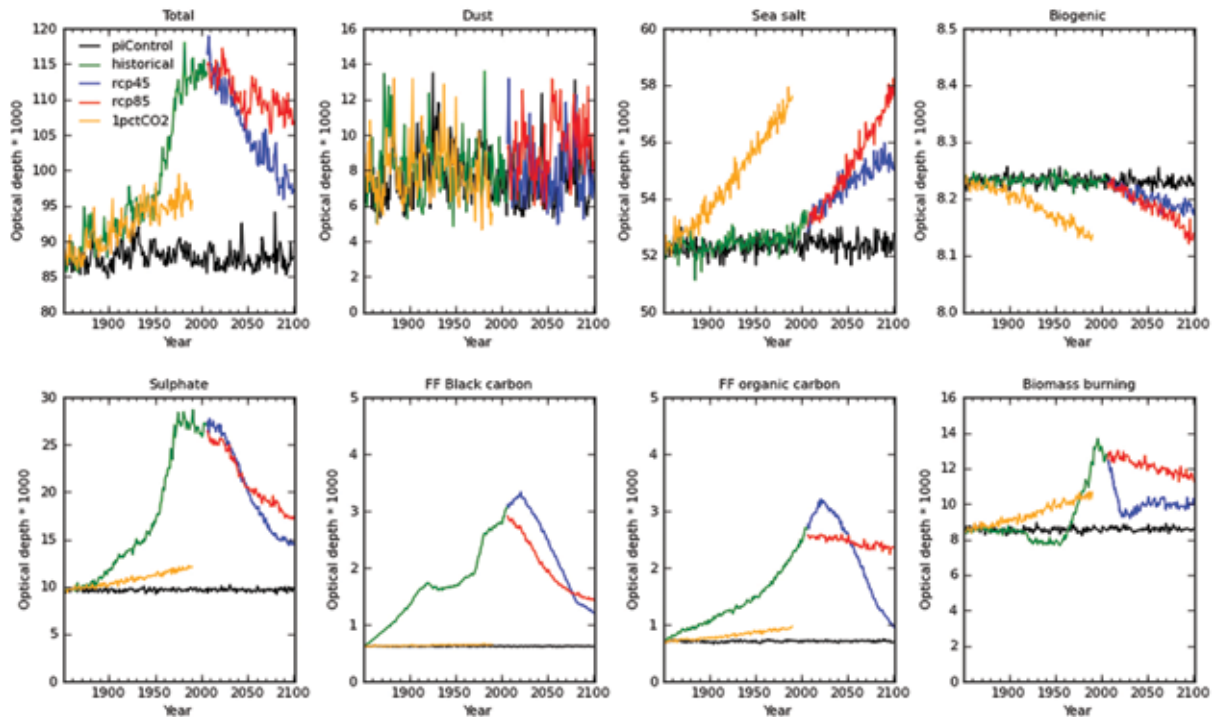
bare soil and depends on wind speed, soil makeup (clay, silt, sand) and soil moisture content. As discussed further below, the global dust burden in ACCESS1.0 is at the lower end of the range of models considered in the AeroCom dust assessment (Huneeus et al. 2011). Dust concentrations in the ACCESS1.3 CMIP5 runs, however, are essentially zero because the model version used was frozen before the dust uplift parameterisation could be adapted for compatibility with the CABLE land-surface scheme. The lack of dust in the ACCESS1.3 CMIP5 runs will have some impact on the model climatology (e.g. Martin and Levine 2012); assessing this impact will be possible once dust uplift in ACCESS1.3 has been optimised.

Aerosol-related emissions specified for CMIP5 scenarios are described by Lamarque et al. (2010, 2011). Emission data files used for the ACCESS CMIP5 runs (for SO_2, land-based DMS, FFOC, FFBC and biomass-burning aerosols) interpolated to the model horizontal grid were obtained from the UK Met Office. The preindustrial control runs used the 1850 values of these emissions.

Consistent with Bellouin et al. (2011), industrial and energy-related SO_2 emissions are included either at the surface or at 500 m (to represent chimney-level emissions). Land-based DMS emissions are included at the surface, FFOC and FFBC emissions are injected at 80 m, and biomass-burning emissions are either at the surface (grass fires) or spread across the boundary layer (forest fires). DMS emissions from seawater are calculated from a climatology of ocean-surface water DMS concentrations (Kettle et al. 1999).

Natural emissions from outgassing volcanos are represented in the CLASSIC scheme using a time-invariant 3D tropospheric source of SO_2 with a total emission rate of ~7.4 Tg[S]y^{-1} (Andres and Kasgnoc 1998). These background tropospheric volcanic emissions of SO_2 were included in all ACCESS CMIP5 runs. The separate effect of stratospheric volcanic aerosols from larger explosive eruptions has been outlined earlier.

Table 1 and Table 2 summarise key aerosol-related quantities from the ACCESS CMIP5 simulations. Results are based on five-year mean global averages centred around 1860 and 2000 for the historical simulations and around 2090 for the RCP8.5 simulations. Values from the ACCESS model are compared with corresponding HadGEM2-ES results from Bellouin et al. (2011) and with annual-mean values from the AeroCom-Median dataset based on a multi-model-median for simulations consistent with year 2000 conditions (Textor et al. 2006).

Consider first the ACCESS1.0 and HadGEM2-ES results shown in Table 1. For non-dust aerosols the ACCESS1.0 and HadGEM2-ES burdens, optical depths, lifetimes and dry deposition fractions are quite similar. This is perhaps not surprising given that the atmospheric components of these models are based on similar configurations of the Unified Model (Bi et al. 2013) and both use the CLASSIC aerosol scheme. That said, the interactive tropospheric chemistry and dynamic vegetation schemes in HadGEM2-ES will cause some differences in aerosol-related quantities including oxidation rates in the sulphur cycle, dry deposition rates and dust emissions. For dust aerosols, ACCESS1.0 has

Table 1. Aerosol optical depths and global burdens in ACCESS1.0 and ACCESS1.3 CMIP5 historical simulations compared with HadGEM2-ES results from Bellouin et al. (2011) and AeroCom-median values. ACCESS and HadGEM2 results are based on global-mean five-year mean quantities for the time period 1998–2002. AeroCom-median optical depths were obtained by globally averaging datasets obtained from the AeroCom database server (http://aerocom.met.no/data.html) and AeroCom-median burdens are from Textor et al. (2006). Burdens for sulphate aerosol (SO_4) are based on the mass of S and those for carbonaceous aerosols (BB, FFOC, FFBC) are based on the mass of C.

Quantity[a]	ACCESS1.0	ACCESS1.3	HadGEM2-ES	AeroCom-Median[d]
AOD (550 nm), 2000				
AER	0.1142	0.1023	0.169	0.112
SO4	0.0264	0.0222	0.024	0.032
BB	0.0129	0.0088	0.012	0.015[d]
FFOC	0.0025	0.0019	0.002	–
FFBC	0.0028	0.0020	0.003	0.003[d]
SS	0.0533	0.0590	0.053	0.026
DU	0.0080	–	0.060	0.023
biogenic[b]	0.0082	0.0083	0.008	
nitrate[c]	n/a	n/a	0.007	
Burden (Tg), 2000				
SO4	0.562	0.431	0.5	0.66
BB	0.954	0.640	0.9	1.76[d]
FFOC	0.193	0.149	0.2	–
FFBC	0.278	0.196	0.3	0.21[d]
DU	8.786	–	45.0	20.5[e]
biogenic	1.129	1.128	1.1	

[a]Aerosols are identified as: AER = total aerosol; SO4 = non-sea salt sulphate; BB = biomass burning; FFOC = fossil-fuel organic carbon; FFBC = fossil fuel black carbon; SS = sea salt; DU = mineral dust; biogenic = a representation of secondary-organic aerosols from terpene emissions from vegetation based on a climatology of monthly-averaged fields obtained using the terpene-oxidation capability within the STOCHEM chemistry-transport model (Derwent et al. 2003); and nitrate = nitrate aerosols as included in some of the HadGEM2-ES simulations of Bellouin et al. (2011) – but not included in ACCESS CMIP5 simulations.
[b]Although biogenic aerosols in the CLASSIC scheme are determined by a climatology, their optical properties depend on humidity, resulting in projected global-mean biogenic AOD (550 nm) decreasing by ~1 per cent from 2000 to 2100 (as seen in Fig. 4 and noted by Bellouin et al. (2011))
[c]Nitrate aerosols were included in some, but not all, of the HadGEM2-ES simulations discussed by Bellouin et al. (2011). The HadGEM2-ES results shown here in Table 1 are for runs which included nitrate aerosols.
[d]AeroCom-median values reported in the BB rows are for particulate organic matter (POM), while those reported in the FFBC rows are for AeroCom's BC (from fossil fuels and biofuels). The different aerosol definitions used by the CLASSIC Aerosol Scheme and the AeroCom assessments makes a direct comparison difficult. When comparing HadGEM2 model results with observations of POM, Collins et al. (2008) used BB + OCFF + biogenic to estimate model POM.
[e]A more recent discussion of AeroCom-Model dust parameters can be found in Huneeus et al. (2011), where the AeroCom-Median burden is given as 15.8 Tg and the global-annual-mean AOD (550 nm) is 0.023. Differences in values reported in the literature for AeroCom-Median quantities may result from the use of different subsets of models to calculate the median and may also reflect the use of different latitude ranges when calculating global annual averages.

a global burden about five times smaller than HadGEM2-ES and a global-mean optical depth about seven times smaller. This is consistent with the over-estimation of dust by the HadGEM2-ES model which has been documented by Bellouin et al. (2011) and Martin and Levine (2012). Dust emissions are both uncertain and highly variable (Zender et al. 2004). The spread of model estimates from the AeroCom study for the global dust burden is 6.8–29.5 Tg and for global-mean AOD (550 nm) it is 0.010–0.035 (Huneeus et al. (2011), global-annual means for year 2000 conditions). Total dust amounts and optical depths in the ACCESS1.0 model are at the lower end of the range of models considered in the AeroCom dust assessment. Although a detailed comparison of ACCESS CMIP5 aerosols with available regional and seasonal observations is beyond the scope of this introductory analysis, the global distribution of the

total AOD can be used to further document aerosols in the ACCESS models.

Figure 5 shows total aerosol optical depths at 550 nm for five-year means centred around the year 2000 for ACCESS1.0 and ACCESS1.3 CMIP5 historical simulations, together with multi-annual-mean distributions from MODIS satellite observations and AeroCom-median values for year 2000 conditions. Corresponding results for HadGEM2-ES can be seen in Fig. 9 of Bellouin et al. (2011). Optical depths in the ACCESS models capture many of the broad features seen in the satellite measurements, although low dust amounts in these models lead to smaller AODs over parts of Africa, central Asia, the Arabian Peninsula, Australia and the mid Atlantic. Between 40°S and 60°S, where SS dominates, ACCESS1.3 has larger total AODs than ACCESS1.0. The mean SS optical depth in this latitude band is 0.112 for

Table 2. Aerosol-related quantities in ACCESS1.0 and AC-CESS1.3 CMIP5 compared with HadGEM2-ES results from Bellouin et al. (2011). Values reported in the table are based on global-mean five-year mean quantities for time periods 1858–1862 and 1998–2002 for the CMIP5 historical scenario and for 2088–2092 for the RCP8.5 scenario. Burdens for sulphate aerosol (SO4) and emissions for its precursor SO_2 are based on the mass of S.

Quantity[a]	ACCESS1.0	ACCESS1.3	HadGEM2-ES[c]
Emissions (Tgy^{-1}), 2000			
SO_2	61.2	61.1	60.3
BB	26.2	26.3	25.9
FFOC	13.0	12.9	12.7
FFBC	5.3	5.2	5.2
DU	2371	–	8192
Lifetime (d), 2000			
SO4	3.5	2.7	3.3
BB	8.3	5.6	7.8
FFOC	5.6	4.3	5.2
FFBC	19.2	13.6	18.1
DU	1.4[d]	–	2.0
% Dry deposition, 2000			
SO4	12.6	16.5	12.0
BB	10.8	24.2	11.8
FFOC	16.4	22.5	18.4
FFBC	20.9	31.6	24.1
DU	88.5	–	81.9
ΔAOD (550 nm), 2000–1860, historical simulation			
AER	0.0263	0.0211	0.031[c]
SO4	0.0166	0.0151	0.015
BB	0.0044	0.0024	0.0042
FFOC	0.0017	0.0012	0.0016
FFBC	0.0021	0.0015	0.0021
SS	0.0011	0.0009	0.0007
DU	0.0004	–	–
biogenic[b]	0.0000	0.0000	0.0
ΔAOD (550 nm), 2090–2000, RCP8.5 simulation			
AER[d]	–0.0060	–0.0058	0.003[c]
SO4	–0.0088	–0.0089	–0.0081
BB	–0.0013	–0.0008	–0.0013
FFOC	–0.0001	–0.0002	–0.0001
FFBC	-0.0013	–0.0011	–0.0014
SS	0.0040	0.0053	0.005
DU	0.0017	–	–
biogenic[b]	–0.0001	–0.0001	–0.0001

[a]Aerosols are identified as: AER = total aerosol; SO4 = non-sea-salt sulphate; BB = biomass burning, FFOC = fossil fuel organic carbon; FFBC = fossil fuel black carbon; SS = sea salt; DU = mineral dust; biogenic = a representation of secondary-organic aerosols from terpene emissions from vegetation based on a climatology of monthly-averaged fields obtained using the terpene-oxidation capability within the STOCHEM chemistry-transport model (Derwent et al. 2003).

[b]Although biogenic aerosols in the CLASSIC scheme are determined by a climatology, their optical properties depend on humidity, resulting in projected global-mean biogenic AOD (550 nm) decreasing by ~1 per cent from 2000 to 2100 (as seen in Fig. 4 and noted by Bellouin et al. (2011))

[c]ΔAOD (550 nm) values for HadGEM2-ES reported in Table 2 are from Bellouin et al. (2011) for simulations which do not include nitrate aerosols. The total-aerosol ΔAOD (550 nm) is for five-year global-mean averages centered around 1860 and 2000. ΔAOD (550 nm) values for individual aerosols are estimated from time-series plots of annual-mean global-mean AOD in Fig. 7 of Bellouin et al. (2011) as the difference between 2000 and 1860. Values for dust are omitted because annual variability in dust AOD was too large for a reasonable estimate to be made so that the total-aerosol ΔAOD (550nm) is not the same as the sum of the listed components.

[d]Changes in total AOD (550 nm) between 1860 and 2000 shown in the table can be compared with the anthropogenic ΔAOD (550 nm) of 0.043 obtained by Bellouin et al. (2008) from an analysis of daily MODIS/Terra data from 2002 using estimated anthropogenic fractions. Bellouin et al. (2008) note that the comparison with model results is sensitive to whether the satellite data mask is used when averaging model data—obtaining ΔAOD (550 nm) = 0.030 without using the mask and 0.040 when using the same mask for HadGEM2-A differences between 1850 and the present. Similar considerations will apply when comparing model results with satellite-based annual-mean AOD distributions such as those shown in Fig. 5 of the present work, so that detailed quantitative comparisons would ideally be carried out using the appropriate latitude-dependent satellite-data masks when averaging the model results.

ACCESS1.0 and 0.129 for ACCESS1.3. The reason for this difference is the higher relative humidity in ACCESS1.3, resulting in larger particles and optical depths because of hygroscopic growth (Yu et al. 2012, Yue and Liao 2012).

Changes in total AOD from 1860 to 2000 for the ACCESS models are also shown in Fig. 5. These regional changes reflect increased anthropogenic emissions from industrialisation, fossil fuel use and biomass burning, as indicated for ACCESS1.0 by the green curves in Fig. 4. In addition to this, dust variability as well as the response of dust uplift and sea salt aerosols to a changing climate may also contribute to calculated AOD changes. Such effects, which lead to the increasing SS AODs seen in Fig. 4, have been discussed by Bellouin et al. (2011) for the HadGEM2-ES model, where it was noted that sea-ice reductions and increased wind speeds result in more sea salt production in a warming climate. The global-average anthropogenic increase in total AOD from 16 AeroCom Phase II models has a mean values of 0.0295, with a standard deviation of 0.011 (Myhre et al. 2013). Corresponding values from ACCESS1.0 and ACCESS1.3 are 0.026 and 0.021, respectively, which are both within one standard deviation of the mean of the models considered in the AeroCom Phase II intercomparison.

Compare the aerosol differences between ACCESS1.0 and ACCESS1.3 given in Table 1. The global-mean sea salt optical depth is larger in ACCESS1.3, consistent with the higher total AODs between 40°S and 60°S seen in Fig. 5 which have been discussed previously. Dust in the ACCESS models has also been considered above. For the other aerosol components, the ACCESS1.0 global mean optical depths are greater than in ACCESS1.3, with differences ranging from 18 per cent for SO$_4$ to 45 per cent for BB. Given that aerosol emissions for SO$_4$ precursors, FFOC, FFBC and BB are the same for both ACCESS models, the reason for the different burdens

Fig. 5.   Annual-mean total AODs at 550 nm for present day conditions (a–d) and AOD changes from 1860 to 2000 (e,f). ACCESS model results are based on five-year means centred around 1860 or 2000 for CMIP5 historical simulations. AeroCom-median AODs are for Experiment A year 2000 conditions and were obtained by averaging monthly-mean data obtained from the AeroCom database server (http://aerocom.met.no/data.html) (dataset: AEROCOM_MEDIAN.monthly.OD550AER.2000. nc). AODs from MODIS (550 nm) satellite observations are based on data from the Giovanni online data system developed and maintained by the NASA Goddard Earth Sciences Data and Information Services Center (Acker and Leptoukh 2007). The MODIS plot is based on Version 5.1 Level 3 monthly data and was obtained by first merging MODIS Dark Target (DT) and MODIS Deep Blue (DB) AODs and then time-averaging the merged monthly data, ignoring missing values (datasets: MYD08_M3.*.051.*.GC.nc). When merging: DT values are used where available; if DT values are negative and BD values exist, (DT + DB) / 2 is used; if DT values are missing, DB values are used, if available. For further information about the MODIS data see Kahn et al. (2011), Levy et al. (2010, 2013) and Remer et al. (2008).
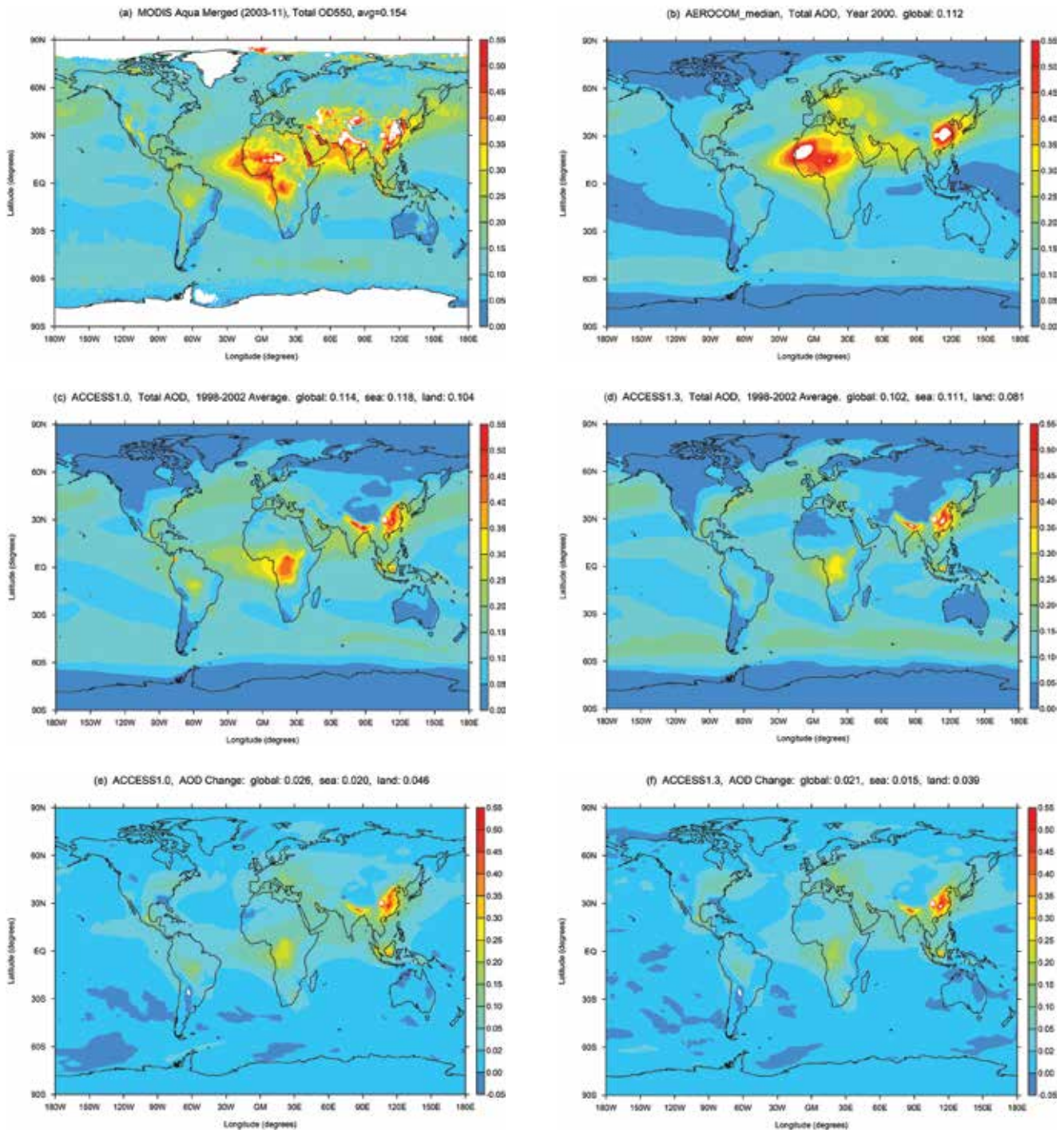
and optical depths must be related to loss processes. This is borne out in the lifetimes (Table 2), with ACCESS1.3 having considerably shorter lifetimes, as expected. A further clue can be found in the dry deposition rates. For ACCESS1.3, dry deposition accounts for a larger percentage of the total deposition than for ACCESS1.0. The largest change in the dry deposition fraction is seen for biomass-burning aerosols, increasing from 11 per cent of the total deposition in ACCESS1.0 to 24 per cent in ACCESS1.3. These changes are driven by increases in the effective first-order dry deposition rates which depend on the properties of the boundary layer and on the land-surface schemes used by the models (MOSES vs CABLE). Upon further investigation, an issue was identified in CABLE-UM interface code which resulted in spuriously large dry deposition rates over some tropical forests in the ACCESS1.3 model. The smaller total AODs in ACCESS1.3 over parts of South America, central Africa and Indonesia seen in Fig. 5 are related to this. Atmosphere-only test runs show that correcting the dry deposition leads to a 13 per cent increase in the global-mean BB AOD but has only a small impact on other aerosols, indicating that other differences in the boundary layer properties between ACCESS1.3 and ACCESS1.0 are responsible for the smaller aerosol burdens calculated by ACCESS1.3.

We return now to a closer examination of the ACCESS1.0 optical-depth time series shown in Fig. 4. Although the one per cent/year CO_2 simulation has the same constant aerosol related emissions as the control, it is included here to illustrate the feedback of changing climate on the aerosol. The temperature at the end of this run is similar to that in the RCP8.5 simulation at 2100 (red curves in Fig. 4). SS is a natural aerosol but, as discussed previously, it depends on climate via changes in wind-speed, humidity and sea-ice extent. While the increase in SS AOD is relatively small (~12 per cent), the magnitude of this change is about 60 per cent of the total AOD increase in the one per cent/year CO_2 run. In the case of the RCP8.5 scenario, the magnitude of the SS AOD increase between 2000 and 2100 is ~65 per cent of the total AOD decrease between 2000 and 2090 for ACCESS1.0 and ~90 per cent of the total AOD decrease for ACCESS1.3. Such SS increases will partly offset warming from increased CO_2 and may also impact on the aerosol-indirect effects (Korhonen et al. 2010).

With the exception of dust and its influence on the total optical depth, the evolution of the optical depths for the historical run and for RCPs 4.5 and 8.5 is qualitatively similar to that shown in Fig. 7 of Bellouin et al (2011). This is consistent with the agreement seen in Table 1 for the five-year mean total AODs noted previously. Results for ACCESS1.3 (not shown) have a similar shape in time, although the overall magnitudes are smaller for SO_4, FFOC, FFBC and BB because of the smaller burdens and shorter lifetimes noted above. The time evolution of the optical-depth profiles is determined primarily by the relevant emission profiles, but is also affected by changes in aerosol residence times as the climate changes. Such residence-time variations have been discussed by Bellouin et al (2011) for the HadGEM2-ES model where it was shown that residence times for SO_4, FFOC, FFBC and BB increase throughout most of the 21st century for RCP4.5 and RCP8.5, by amounts varying from a few percent to over 50 per cent for FFOC, in response to changing precipitation and wet-deposition rates. Variations in aerosol residence times can also be expected in the ACCESS simulations, with the details depending on the land-surface scheme, the cloud treatment, and the relative contribution from wet deposition.

Although ACCESS1.3 has 20 per cent less sulphate aerosol than ACCESS1.0, it is not clear without further experimentation what the difference in aerosol radiative forcing will be, direct or indirect. For example, ACCESS1.3 has significantly more low cloud than ACCESS1.0 (Bi et al. 2013) which may affect the aerosol forcing. Any difference here will have opposite effects in the historical and RCP simulations because aerosol amounts increase in the former and decrease in the latter. CMIP5 includes a prescribed method for calculation of the net radiative forcing due to anthropogenic aerosols. This is based on a pair of atmospheric model simulations with prescribed sea surface temperatures; one using aerosol and precursor emissions for 1850, with the other using emissions for 2000 (Taylor et al. 2009). These experiments with the ACCESS models are under way and will be reported in a subsequent paper.

Historical simulations and 21st century climate projections using RCPs

This paper presents results from the CMIP5 idealised and climate projection simulations with a focus on changes in surface air temperature and the hydrologic cycle, and on climate sensitivity. Further details of the atmospheric changes are shown by Rashid et al. (2013), and results for the ocean and sea-ice changes are presented by Marsland et al. (2013), and Uotila et al. (2013).

Although the ACCESS models have a relatively small drift in the control simulations, for a proper comparison with observed temperature change this should be removed (e.g. Sen Gupta et al. 2012). Here we use the linear trend in global mean temperature over the full 500 years of the control runs. This is 0.065 K/century in ACCESS1.0 and 0.0067 K/century in ACCESS1.3 (Bi et al. 2013).

Figure 6 shows the global annual mean surface air temperature anomalies from the historical simulations compared to observations (Brohan et al. 2006). Both models and observations show significant warming since about 1965, with ACCESS1.0 showing a slightly larger trend than ACCESS1.3.

Although both models capture the warming since the 1960s, they do not simulate the warming observed from 1910 to 1940. Both models show a large sustained cooling in the late 19th century following the Krakatoa eruption. This apparent response is much stronger than seen in the observations. Several other CMIP5 models also show a

Fig. 6. Global annual mean surface air temperature anomaly relative to the 1880–1920 mean from the ACCESS historical runs (extended to 2010 using the RCP4.5 simulations) and from observations (Brohan et al. 2006). Solid line is smoothed with a 21 point binomial filter. Dashed sections show where smoothing uses data extended with repetition of end values.
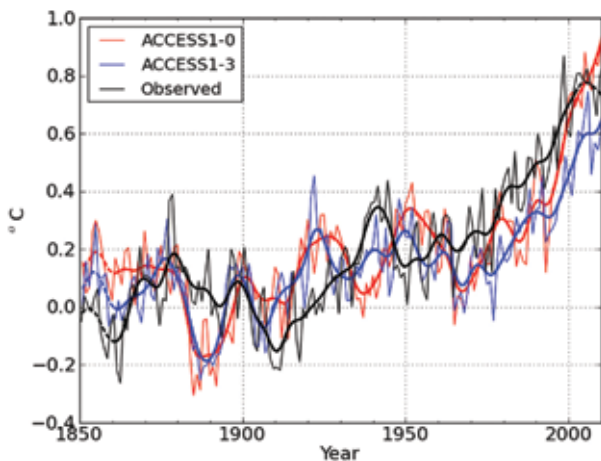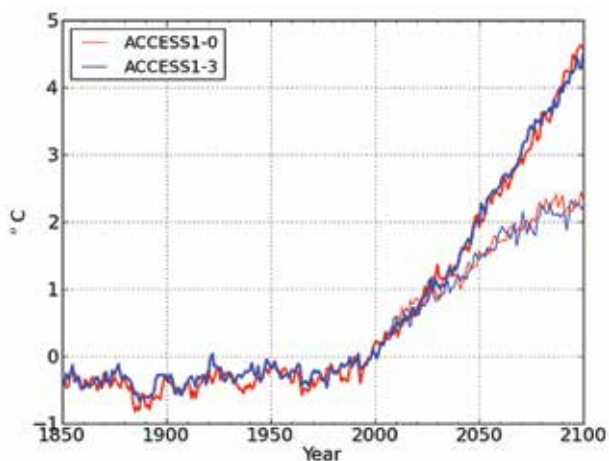

Fig. 7. Time series of annual globally averaged surface air temperature anomalies (relative to 1986–2005 base period) for ACCESS1.0 (red) and ACCESS1.3 (blue) historical and RCP simulations. Heavy line is RCP8.5 and light line is RCP4.5. In each case the control drift has been removed.

similarly strong cooling (Gent et al. 2011, Watanabe et al. 2011, Dufresne et al. 2013, Forster et al. 2013).

Figure 7 shows time series of global average surface air temperature changes from both ACCESS1.0 and ACCESS1.3 from the historical, RCP4.5 and RCP8.5 simulations. The simulations of warming during the 21st century are remarkably similar in the two models (see later for more on climate sensitivity). Aerosol concentrations peak around the present time (2010) and so aerosol changes are a negative radiative forcing in the historical simulations, but a positive radiative forcing relative to the present in the RCP simulations. Without an ensemble of historical simulations it is not clear whether the differences in the model warming

rates at the end of the 20th century (1990–2010) seen in Fig. 6 are the result of true differences in the models' underlying climate sensitivities or are more due to natural variability.

Mean warming (relative to 1986–2005) for the last 20 years of the RCP8.5 simulations is +3.61 K and +3.56 K for ACCESS1.0 and ACCESS1.3 respectively. For the RCP4.5 simulations it is +2.34 K and +2.12 K respectively. The RCP4.5 simulations show some sign of temperature stabilisation by 2100, but the temperature in the RCP8.5 experiments continues to increase almost linearly (as do the CO_2 concentrations).

Figure 8 shows the patterns of normalised temperature change (local difference relative to global mean difference) at the end of the 21st century for both models and both scenarios. This pattern scaling has been widely used for comparing changes across models and scenarios, particularly in the climate impact community (e.g. Mitchell 2003, Watterson and Whetton 2011, Ishizaki et al. 2012). Here the overall patterns are very similar with land generally warming more than ocean, except for the Arctic ocean where warming is largest due to sea-ice retreat (see Marsland et al. 2013). In the RCP85 simulation the ratio of land mean warming to the global mean is 1.44 in ACCESS1.0 compared to 1.32 in ACCESS1.3 and the ratios are similar in the RCP45 simulations.

Figure 9 shows time series of the percentage change in global average precipitation relative to the 1986–2005 base period. In contrast to global mean temperature where there was little difference between the models, here the precipitation increase is markedly larger in ACCESS1.3. The global precipitation change is dominated by changes over the oceans, suggesting that the difference in land surface models is not responsible. However ACCESS1.3 does also show a larger increase in land average precipitation than ACCESS1.0. Both models show a decrease in precipitation during the historical run, up until about 1990. The increase in precipitation starts later than the increase in temperature shown in Fig. 6.

There have been many analyses of the correlation between global precipitation and temperature anomalies, using both observations and models. The relation is usually expressed in terms of the 'hydrological sensitivity', the percentage precipitation change per degree of warming. Held and Soden (2006) found a rate of around 2 per cent/K using CMIP3 simulations with the SRESA1B scenario. Frieler et al. (2011) found an overall sensitivity of 2.2 per cent/K, again analysing CMIP3 simulations. However models that included black carbon aerosol forcing showed considerable variation in the hydrological sensitivity between different scenarios while models without this forcing showed little variation. HadGEM1 was found to have a negative sensitivity over the 20th century, and a smaller sensitivity in the SRES A2 scenario experiment compared to SRES B1 over the 21st century. Shiogama et al. (2010a) also found this was common across CMIP3 models with the largest sensitivity values associated with in SRES B1 experiments and the smallest in

Fig. 8.   Normalised temperature change for (2081–2100)–(1986–2005). This is the local temperature difference scaled by the global mean temperature difference.
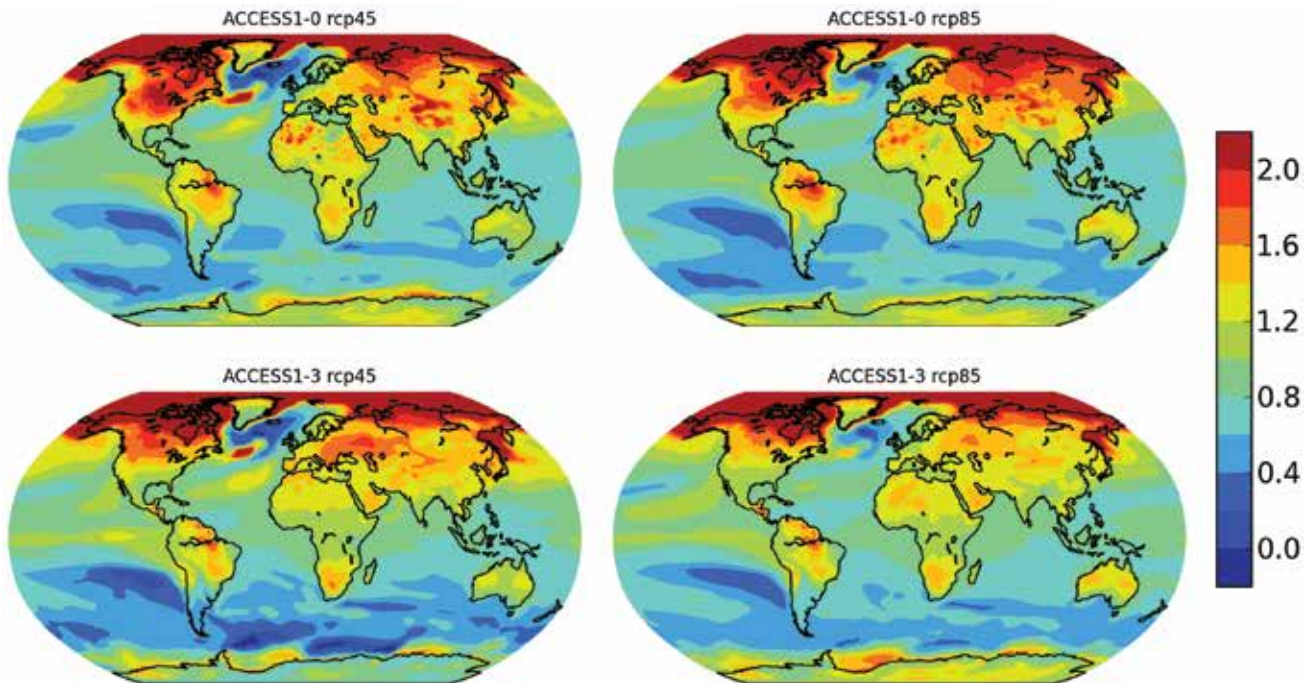
A2. They attributed this to differences in aerosols. A more detailed study with the (CMIP3) MIROC3.2 model found that black and organic carbon aerosols were mainly responsible for such differences (Shiogama et al. 2010b). Andrews et al. (2010) also studied the precipitation response of models to a number of different individual forcings and found a range from –0.24 to 3.5 per cent/K.

Table 3 gives the precipitation change scaled by the global mean temperature change for the end of the 21st century. As in Fig. 9, both models show a larger relative precipitation increase in RCP4.5 than RCP8.5. The hydrological sensitivity of ACCESS1.3 is markedly larger than ACCESS1.0. Many studies have shown that the precipitation response is controlled by changes in the net radiative balance of the atmosphere (e.g. Vecchi and Soden 2007, Bala et al. 2009, Andrews et al. 2010). Figure 10 shows that this close relation also holds in the ACCESS RCP simulations. However in ACCESS1.3 the net atmospheric radiation is more sensitive to temperature change than in ACCESS1.0, so the precipitation also increases more with temperature. This difference in radiative behaviour is predominantly in the long-wave term but further work is required to separate the roles of cloud, water vapour and lapse rate feedbacks.

Figure 11 shows the geographical distribution of the normalised rainfall change. The differences of order one percent/degree in global means are not obvious here because regional differences are much larger. Both models show large rainfall increases in the tropical Pacific, but in ACCESS1.3 this is stronger and extends further to the west. Precipitation over northern hemisphere mid latitudes is also generally larger in ACCESS1.3. Both models show rainfall decreases

Fig. 9.   Time series of percentage change in annual globally averaged precipitation (relative to 1986–2005 base period) for ACCESS1.0 (red) and ACCESS1.3 (blue) historical and RCP simulations. Heavy lines are RCP8.5 and light lines are RCP4.5.
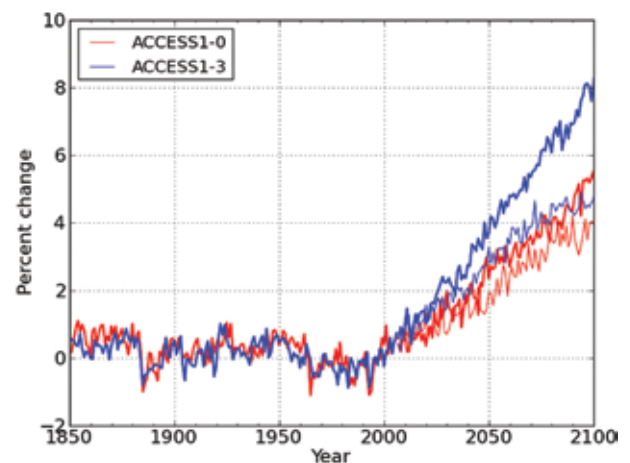

Table 3.   Percentage change in global annual precipitation (2081–2100) relative to (1986–2005) scaled by temperature change (per cent/K).

Model	RCP4.5	RCP8.5
ACCESS1.0	1.60	1.13
ACCESS1.3	2.09	1.80

Fig. 10.   (a) Correlation between changes in annual means of global-mean net atmospheric radiation and precipitation in the RCP45 (circles) and RCP85 (triangles) experiments with ACCESS1.0 shown in red and ACCESS1.3 in blue. (b) As for (a), except showing the relationship between atmospheric radiation and surface air temperature.
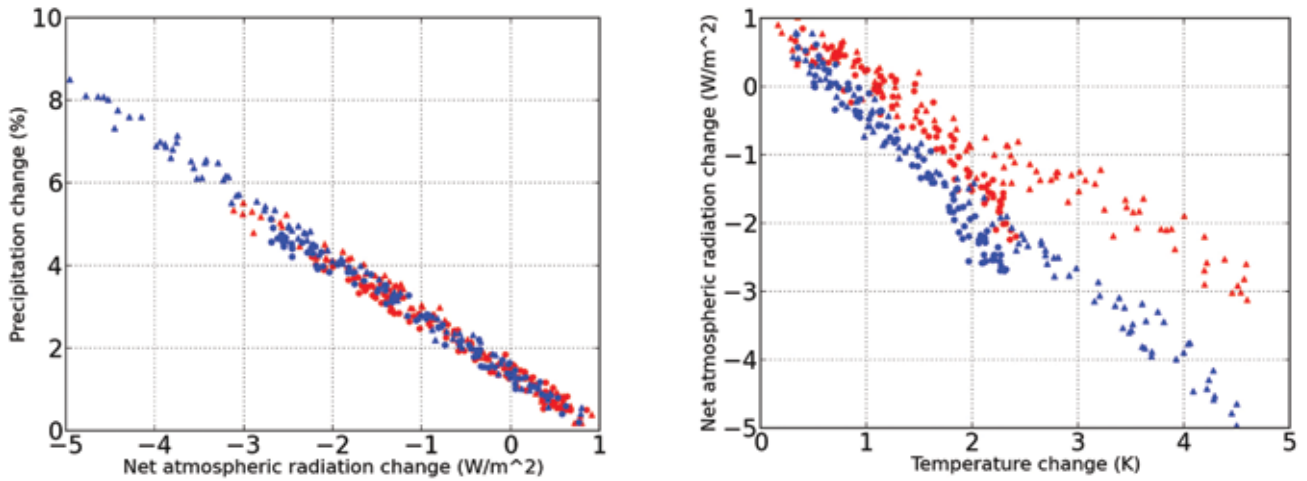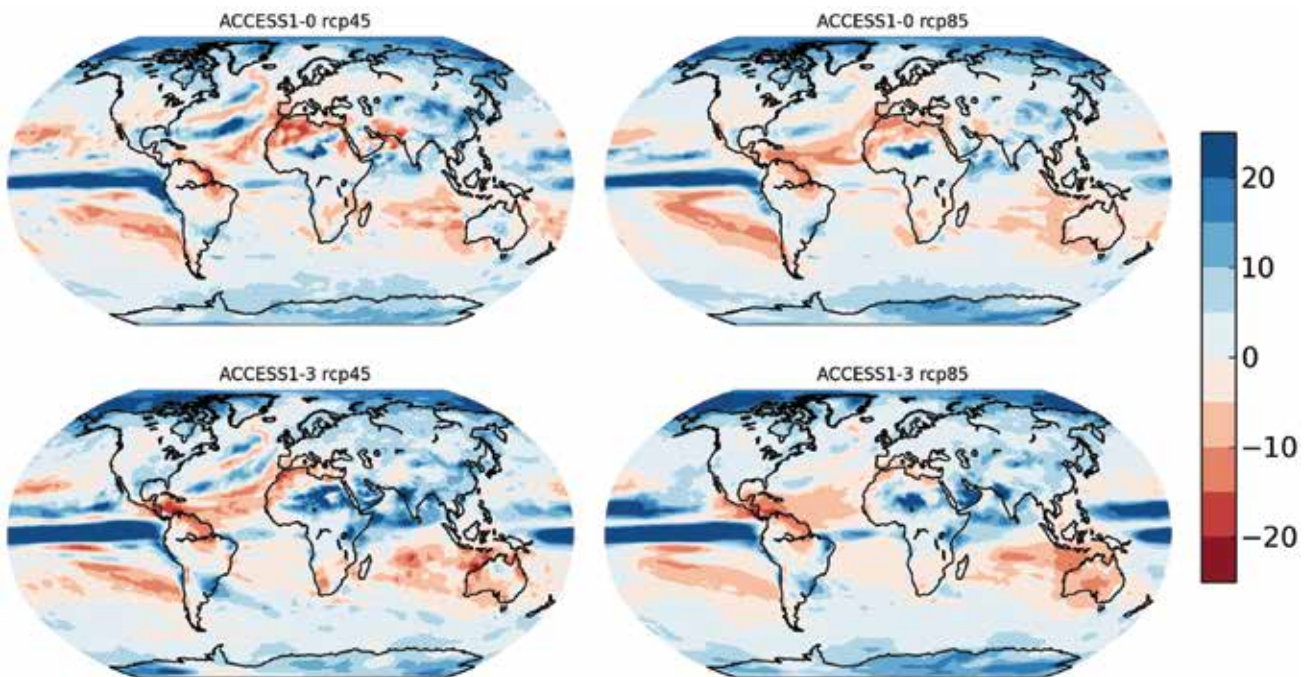

Fig. 11.   Normalised precipitation change for (2081–2100)–(1986–2005) for both models and both RCP scenarios. Units are per cent/K.

in the subtropics, particularly in the southern hemisphere. In both scenarios there is a larger decrease in rainfall to the northwest of Australia in ACCESS1.3 and a larger decrease in rainfall over much of the Australian continent in this model. This is consistent with the relationship between 21st century changes in Australian rainfall and a Pacific-Indian Ocean sea-surface temperature dipole index found by Watterson (2011) in a multi-model analysis of CMIP3 simulations. In ACCESS1.3 the west Pacific warms more than the Indian Ocean whereas warming rates are similar in ACCESS1.0.

## Idealised experiments and climate sensitivity

In addition to the historical and scenario experiments, the CMIP5 experimental design includes a number of idealised diagnostic experiments designed to help understand the differences in model response. These use only specified CO_2 concentrations with all other forcings held constant.

Historically, the main parameter of interest has been the equilibrium climate sensitivity (ECS), defined as the equilibrated warming in a doubled CO_2 experiment with a mixed layer ocean (see Knutti and Hegerl 2008 for a history of climate sensitivity). These models achieved

Table 4. Feedback parameters derived from linear regression. Ranges (second line of entries) are the 2.5–97.5 per cent confidence interval. HadGEM2-ES results, model mean (15 CMIP5 models) and standard deviation (SD) are from Andrews et al. (2012).

Model	Forcing (4 x CO_2)	Net	LW clear	SW clear	LW CRE	SWCRE	NetCRE	ECS $2 \times CO_2$
		Climate feedback parameter						
ACCESS1.0	5.88 5.3, 6.3	–0.76 –0.85, –0.64	–1.62	0.75	0.08	0.03	0.11	3.86 3.71, 4.13
ACCESS1.3	5.77 5.2, 6.2	–0.81 –0.91, –0.67	–1.83	0.75	–0.13	0.40	0.27	3.54 3.39, 3.82
HadGEM2-ES	5.85	–0.64	–1.66	0.65	0.12	0.25	0.37	4.59
Model mean	6.89	–1.08	–1.83	0.72	0.06	–0.04	0.02	3.37
Model SD	1.12	0.29	0.13	0.11	0.18	0.38	0.32	0.83

Fig. 12. Global annual mean surface temperature change (heavy line) and net TOA flux change (light line) in the ACCESS1.0 (red) and ACCESS1.3 (blue) abrupt 4 x CO_2 experiments.
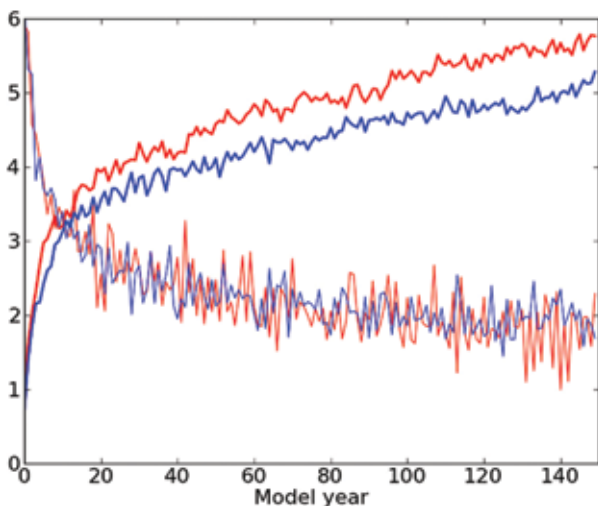
equilibrium within a reasonable time, of order decades. With dynamic ocean models, reaching equilibrium may take several thousand years and is not generally practical (e.g. Stouffer 2004, Li et al. 2012). However the ECS concept is still scientifically useful because it is a large contributor to differences between models. Changes in many model variables scale approximately with global mean temperature and so with the climate sensitivity (e.g. Mitchell 2003).

An alternate measure of climate sensitivity useful for comparing models is the transient climate response (TCR), defined as the warming at time of doubling in a one per cent/year CO_2 experiment (Cubasch et al. 2001). This depends on both the equilibrium model sensitivity and the rate of ocean heat uptake (e.g. Winton et al. 2010). The CMIP5 core idealised experiment used for estimating the TCR involves a one per cent/year CO_2 growth for 140 years, to reach a level four times the base concentration.

The TCR (year 61–80 average) is 1.89 K in ACCESS1.0 and 1.64 K in ACCESS1.3. This difference between the models

is further discussed below. The range of TCR for 19 CMIP3 models was found to be 1.2 to 2.6 K with median 1.6 K (Randall et al. 2007). An analysis of 23 CMIP5 models found a similar range of 1.1 to 2.5 K with median 1.8 K (Forster et al. 2013).

Gregory et al. (2004) introduced the idea of estimating climate sensitivity from the correlation of temperature and energy balance changes which does not require the model to be at equilibrium. This method involves a simulation where the CO_2 is instantaneously elevated and then held constant at the higher level, with the correlation calculated during the initial part of the equilibration process. The CMIP5 core idealised experiment used for estimating the ECS by the Gregory method involves an instantaneous quadrupling of CO_2 concentration which is then held fixed for 150 years (Taylor et al 2011).

The Gregory et al. (2004) approach assumes the response to a constant radiative forcing F is a simple linear relation between the change in the top of atmosphere (TOA) net energy flux N, and the change in the surface air temperature T,

$$N = F - \alpha \, \Delta T,$$

with α (W m^{-2} K^{-1}) the climate feedback parameter. Regressing N and ΔT allows estimation of both the radiative forcing F and α. Note that the forcing calculated here is not the pure CO_2 radiative forcing because it includes short-term atmospheric adjustments other than the stratospheric equilibration (Gregory and Webb 2008).

Andrews et al. (2012) analysed feedbacks from 15 CMIP5 models using this approach. However they did not include ACCESS1.0 or 1.3 because these results were not available at the time of their analysis. Here we present results of this feedback calculation applied to the ACCESS models and compare results with Andrews et al (2012).

Figure 12 shows the global mean surface air temperature change and TOA net radiation change in the ACCESS abrupt 4 x CO_2 experiments. The control drifts in both temperature and net flux (calculated over the full 500 year control runs) have been removed. In this experiment (and in the one per cent/year CO_2 experiments) it is clear that ACCESS1.0

Fig. 13.   Relationship between change in TOA net radiative flux and surface air temperature from first 150 years of the abrupt 4 x CO_2 experiments. Data points are annual global means. Line shows the linear regression fit.
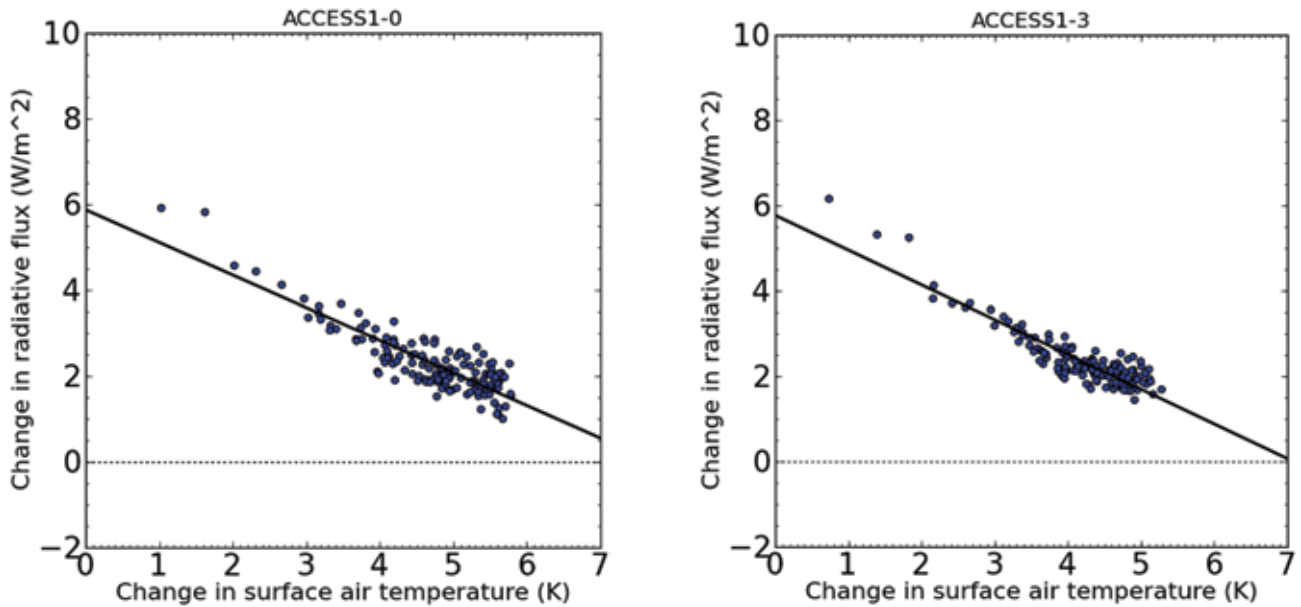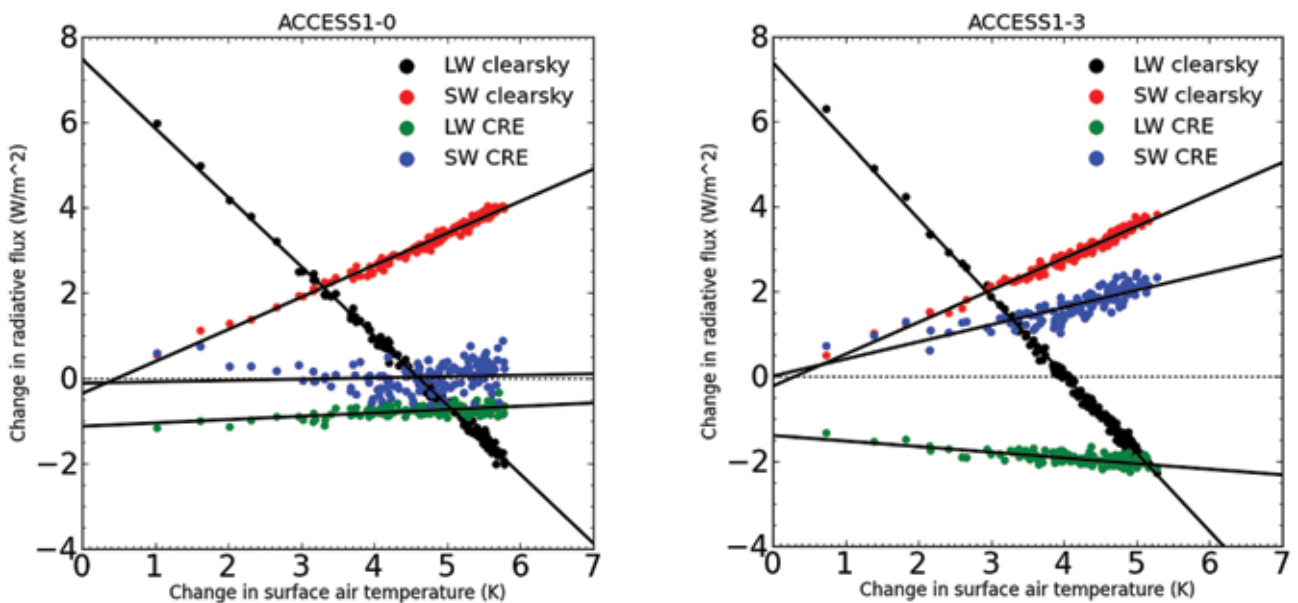

Fig. 14.   As in Fig. 13, except now showing individual flux components.

warms more than ACCESS1.3, in contrast to the historical and RCP experiments where they could not be definitely separated. After 150 years the net TOA flux is still around 2 W m^{-2} and the models are clearly far from equilibrium. In fact, continuing the experiments for a further 200 years (350 in total) still yields a final net flux around 1.5 W m^{-2}.

Figure 13 shows the relationship between the TOA net flux and temperature change for both ACCESS models. The axis intercepts give estimates of the 4 x CO_2 radiative forcing and equilibrium temperature change and the values are given in Table 4. The 2.5–97.5 per cent confidence intervals

were calculated using the same bootstrap sampling method as Andrews et al. (2012). The forcing in ACCESS1.3 is slightly smaller than in ACCESS1.0, though this difference is not significant given the fitting uncertainties. The ECS for doubled CO_2 is 3.86 K in ACCESS1.0 and 3.54 K in ACCESS1.3. This is similar to the relative differences in the transient climate response in the one per cent/year CO_2 experiments given above and so is likely more robust than the regression uncertainties suggest.

The behaviour of the separate LW and SW clear sky fluxes and cloud radiative effects (all sky change minus clear sky

change) are shown in Fig. 14. In ACCESS1.0 the LW and SW cloud radiative effects (CRE) have only a small dependence on temperature. In ACCESS1.3 they have larger and opposite tendencies. Both models show a decrease in total cloud with increasing temperature with the rate of decrease larger in ACCESS1.3. The simple regression calculation is unable to separate the effects of changes in cloud amount and cloud optical properties which would require a radiative perturbation calculation (e.g. Colman and McAvaney 2011). In both models there is a net positive cloud feedback, slightly larger in ACCESS1.3. The LW CRE has an axis intercept of approximately 1 W m^{-2}. A large part of this is likely due to the effect of the clouds masking the CO_2 radiative forcing (Andrews et al. 2011, Colman and McAvaney 2011), emphasising the difference between changes in CRE and true cloud feedback (e.g. Soden et al. 2004).

The sensitivity of both models is above the mean of the 15 models analysed by Andrews et al. (2012). The ACCESS1.0 sensitivity is smaller than the HadGEM2-ES value of 4.59 K despite the similarity of the atmosphere and land surface model components. This suggests the ocean and/or sea-ice components have a significant impact on the climate sensitivity. The main difference appears to come comes from the SW CRE term which is larger in HadGEM2-ES. Further analysis is required to determine to whether this difference is due to different patterns of surface temperature change, different cloud responses or due to other changes that appear different in clear and cloudy regions (e.g. surface albedo).

Conclusions

The two versions of the ACCESS-CM, namely ACCESS1.0 and ACCESS1.3 (Bi et al. 2013), differ mainly in their land surface components and cloud schemes. A preliminary analysis has been conducted of results from both realistic and idealised climate change scenario experiments submitted to CMIP5. The simulations include changes in well mixed GHGs, tropospheric aerosols, ozone, stratospheric aerosol from volcanic eruptions and ozone, according to the CMIP5 experimental design (Taylor et al. 2012). The tropospheric aerosol concentrations and optical depths in ACCESS1.0 (excluding dust) are similar to those in HadGEM2-ES (Bellouin et al. 2011); concentrations of several aerosols in ACCESS1.3 are rather smaller than those in ACCESS1.0.

The temperature changes in the historical simulations from both ACCESS1.0 and ACCESS1.3 models show a late 20th century warming rate broadly similar to that observed, with ACCESS1.0 warming slightly more than ACCESS1.3. Neither version reproduces the observed mid-century warming and the late start to the rapid warming suggests overly strong negative forcing from aerosols. Global mean precipitation decreases up to about 1990 in both historical simulations, again consistent with strong aerosol forcing. However, a proper attribution of this will require an analysis of experiments with individual forcings.

Projected global mean temperatures are very similar in the two models, though land warms relatively more in ACCESS1.0. Patterns of rainfall change are also similar between the two models, though slightly stronger in ACCESS1.3.

Analysis of idealised one per cent/year CO_2 and abrupt 4 x CO_2 experiments show that the basic model sensitivity (transient climate response and equilibrium climate sensitivity) is 10–15 per cent larger in ACCESS1.0 than ACCESS1.3. The transient climate response and equilibrium climate sensitivity for both models are above the medians estimated from multi-model analyses of CMIP3 and CMIP5 results.

The initial analysis in this paper is insufficient to explain the difference in idealised climate sensitivity and what effect it has on the warming in the historical experiments. This will be explored in future research. Extra model runs to form an ensemble of historical simulations and experiments with separate forcings (e.g. GHG only, aerosol only) are planned and will be valuable in understanding these questions.

Full model output has been submitted to the CMIP5 archive and is available for more detailed study and multi-model analyses.

Acknowledgments

References

Andres, R.J. and Kasgnoc, A.D. 1998. A time-averaged inventory of sub-aerial volcanic sulfur emissions. *J. Geophys. Res., 103,* 25251–25261, doi:10.1029/98JD02091.

Andrews, T., P.M. Forster, O. Boucher, N. Bellouin, and A. Jones. 2010. Precipitation, radiative forcing and global temperature change. *Geophys. Res. Lett, 37,* doi:10.1029/2010GL043991.

Andrews, T., J.M. Gregory, P.M. Forster, and M.J. Webb. 2011. Cloud Adjustment and its Role in CO_2 Radiative Forcing and Climate Sensitivity: A Review. *Surv. Geophys.,* doi:10.1007/s10712-011-9152-0.

Andrews, T., J.M. Gregory, M.J. Webb, and K.E. Taylor. 2012. Forcing, feedbacks and climate sensitivity in CMIP5 coupled atmosphere-ocean climate models. *Geophys. Res. Lett, 39,* 1–7, doi:10.1029/2012GL051607.

Bala, G., K. Caldeira, and R. Nemani. 2009. Fast versus slow response in climate change: implications for the global hydrological cycle. *Clim. Dyn., 35,* 423–434, doi:10.1007/s00382-009-0583-y.

Bellouin, N., O. Boucher, J. Haywood, C. Johnson, A. Jones, J. Rae, and S. Woodward. 2007. *Improved representation of aerosols for HadGEM2.* Hadley Centre Tech. Note 73.

Bellouin, N., A. Jones, J. Haywood, and S. A. Christopher. 2008. Updated estimate of aerosol direct radiative forcing from satellite observations and comparison against the Hadley Centre climate model. *J. Geophys. Res., 113,* doi:10.1029/2007JD009385.

Bellouin, N., J. Rae, A. Jones, C. Johnson, J. Haywood, and O. Boucher. 2011. Aerosol forcing in the Climate Model Intercomparison Project (CMIP5) simulations by HadGEM2-ES and the role of ammonium nitrate. *J. Geophys. Res., 116,* 1–25, doi:10.1029/2011JD016074.

Bi, D. and coauthors. 2013. The ACCESS Coupled Model: Description, Control Climate and Preliminary Validation. *Aust. Met. Oceanogr. J., 63,* 41–64.

Brohan, P., J.J. Kennedy, I. Harris, S.F.B. Tett, and P.D. Jones. 2006. Uncertainty estimates in regional and global observed temperature changes: A new data set from 1850. *J. Geophys. Res., 111,* 1–21, doi:10.1029/2005JD006548.

Cionni, I. and coauthors. 2011. Ozone database in support of CMIP5 simulations: results and corresponding radiative forcing. *Atmos. Chem. Phys., 11,* 11267–11292, doi:10.5194/acp-11-11267-2011.

Collins, W.J. and coauthors. 2008. *Evaluation of the HadGEM2 model.* Hadley Centre Tech. Note 74.

Collins, W.J. and coauthors. 2011. Development and evaluation of an Earth-System model – HadGEM2. *Geosci. Model Dev., 4,* 1051–1075, doi:10.5194/gmd-4-1051-2011.

Colman, R.A., and B.J. McAvaney. 2011. On tropospheric adjustment to forcing and climate feedbacks. *Clim. Dyn., 36,* 1649–1658, doi:10.1007/s00382-011-1067-4.

Cubasch, U. and coauthors. 2001. Projections of Future Climate Change. *Climate Change 2001: The Scientific Basis. Contribution of Working Group I to the Third Assessment Report of the Intergovernmental Panel on Climate Change,* Eds. J.T. Houghton, Y. Ding, D.J. Griggs, M. Noguer, P. Van der Linden, X. Dai, K. Maskell, and C.I. Johnson, 525–582, Cambridge University Press.

Derwent, R.G., W.J. Collins, M.E. Jenkin, C.E. Johnson, and D.S. Stevenson. 2003. The Global Distribution of Secondary Particulate Matter in a 3-D Lagrangian Chemistry Transport Model. *J. Atmos. Chem, 44,* 57–95, doi:10.1023/A:1022139814102.

Dufresne, J.-L. and coauthors. 2013. Climate change projections using the IPSL-CM5 Earth System Model: from CMIP3 to CMIP5. *Clim. Dyn.,* doi:10.1007/s00382-012-1636-1.

Essery, R.L.H., M.J. Best, R.A. Betts, P.M. Cox, and C.M. Taylor. 2003. Explicit Representation of Subgrid Heterogeneity in a GCM Land Surface Scheme. *J. Hydrometerol., 4,* 530–543, doi:10.1175/1525-7541(2003)004<0530:EROSHI>2.0.CO;2.

Forster, P. M., T. Andrews, P. Good, J.M. Gregory, L.S. Jackson, and M. Zelinka. 2013. Evaluating adjusted forcing and model spread for historical and future scenarios in the CMIP5 generation of climate models. *J. Geophys. Res., 118,* doi:10.1002/jgrd.50174.

Frieler, K., M. Meinshausen, T. Schneider von Deimling, T. Andrews, and P. Forster. 2011. Changes in global-mean precipitation in response to warming, greenhouse gas forcing and black carbon. *Geophys. Res. Lett., 38,* 1–5, doi:10.1029/2010GL045953.

Fröhlich, C., and J. Lean. 2004. Solar radiative output and its variability: evidence and mechanisms. *Astron. Astrophys. Rev, 12,* 273–320, doi:10.1007/s00159-004-0024-1.

Gent, P.R. and coauthors. 2011. The Community Climate System Model Version 4. *J. Clim., 24,* 4973–4991, doi:10.1175/2011JCLI4083.1.

Gregory, J., and M. Webb. 2008. Tropospheric Adjustment Induces a Cloud Component in CO_2 Forcing. *J. Clim., 21,* 58–71, doi:10.1175/2007JCLI1834.1.

Gregory, J.M. and coauthors. 2004. A new method for diagnosing radiative forcing and climate sensitivity. *Geophys. Res. Lett., 31,* L03205, doi:10.1029/2003GL018747.

Sen Gupta, A., L.C. Muir, J.N. Brown, S.J. Phipps, P.J. Durack, D. Monselesan, and S.E. Wijffels. 2012. Climate Drift in the CMIP3 Models. *J. Clim., 25,* 4621–4640, doi:10.1175/JCLI-D-11-00312.1.

Hansen, J. and coauthors. 2005. Efficacy of climate forcings. *J. Geophys. Res., 110,* doi:10.1029/2005JD005776.

Held, I.M., and B.J. Soden. 2006. Robust Responses of the Hydrological Cycle to Global Warming. *J. Clim., 19,* 5686–5699, doi:10.1175/JCLI3990.1.

Hewitt, H.T., D. Copsey, I.D. Culverwell, C.M. Harris, R.S.R. Hill, A. B. Keen, A.J. McLaren, and E.C. Hunke. 2011. Design and implementation of the infrastructure of HadGEM3: the next-generation Met Office climate modelling system. *Geosci. Model Dev., 4,* 223–253, doi:10.5194/gmd-4-223-2011.

Huneeus, N. and coauthors. 2011. Global dust model intercomparison in AeroCom phase I. *Atmos. Chem. Phys., 11,* 7781–7816, doi:10.5194/acp-11-7781-2011.

Ishizaki, Y. and coauthors. 2012. Temperature scaling pattern dependence on representative concentration pathway emission scenarios. *Clim. Change, 112,* 535–546, doi:10.1007/s10584-012-0430-8.

Jones, A., D.L. Roberts, M.J. Woodage, and C.E. Johnson. 2001. Indirect sulphate aerosol forcing in a climate model with an interactive sulphur cycle. *J. Geophys. Res., 106,* 20293–20310, doi:10.1029/2000JD000089.

Jones, C.D. and coauthors. 2011. The HadGEM2-ES implementation of CMIP5 centennial simulations. *Geosci. Model Dev., 4,* 543–570, doi:10.5194/gmd-4-543-2011.

Kahn, R.A. and coauthors. 2011. Response to 'Toward unified satellite climatology of aerosol properties. 3. MODIS versus MISR versus AERONET'. *J. Quant. Spectrosc. Radiat. Transfer, 112,* 901–909, doi:http://dx.doi.org/10.1016/j.jqsrt.2010.11.001.

Kettle, A.J. and coauthors. 1999. A global database of sea surface dimethylsulfide (DMS) measurements and a procedure to predict sea surface DMS as a function of latitude, longitude, and month. *Glob. Biogeochem. Cycles, 13,* 399, doi:10.1029/1999GB900004.

Knutti, R., and G.C. Hegerl. 2008. The equilibrium sensitivity of the Earth's temperature to radiation changes. *Nature Geosci.,* 735–743.

Kopp, G., and J.L. Lean. 2011. A new, lower value of total solar irradiance: Evidence and climate significance. *Geophys. Res. Lett., 38,* 1–7, doi:10.1029/2010GL045777.

Korhonen, H., K.S. Carslaw, P.M. Forster, S. Mikkonen, N.D. Gordon, and H. Kokkola. 2010. Aerosol climate feedback due to decadal increases in Southern Hemisphere wind speeds. *Geophys. Res. Lett., 37,* 0–5, doi:10.1029/2009GL041320.

Kowalczyk, E.A., Y.P. Wang, R.M. Law, H.L. Davies, J.L. McGregor, and G.S. Abramowitz. 2006. *The CSIRO Atmosphere Biosphere Land Exchange (CABLE) model for use in climate models and as an offline model.* CSIRO Marine and Atmospheric Research paper 013, www.cmar.csiro.au/e-print/open/kowalczykea_2006a.pdf.

Kowalczyk, E.A. and coauthors. 2013. The land surface model component of ACCESS: description and impact on the simulated surface climatology. *Aust. Met. Oceanogr. J., 63,* 65–82.

Lamarque, J.-F. and coauthors. 2010. Historical (1850–2000) gridded anthropogenic and biomass burning emissions of reactive gases and aerosols: methodology and application. *Atmos. Chem. Phys., 10,* 7017–7039, doi:10.5194/acp-10-7017-2010.

Lamarque, J.-F., G.P. Kyle, M. Meinshausen, K. Riahi, S.J. Smith, D.P. Vuuren, A.J. Conley, and F. Vitt. 2011. Global and regional evolution of short-lived radiatively-active gases and aerosols in the Representative Concentration Pathways. *Clim. Change, 109,* 191–212, doi:10.1007/s10584-011-0155-0.

Lean, J.L. 2009. Calculations of Solar Irradiance. http://sparcsolaris.gfz-

potsdam.de/Input_data/Calculations_of_Solar_Irradiance.pdf.

Levy, R.C., L.A. Remer, R.G. Kleidman, S. Mattoo, C. Ichoku, R. Kahn, and T.F. Eck. 2010. Global evaluation of the Collection 5 MODIS dark-target aerosol products over land. *Atmos. Chem. Phys., 10,* 10399–10420, doi:10.5194/acp-10-10399-2010.

Levy, R.C., S. Mattoo, L.A. Munchak, L.A. Remer, A.M. Sayer, and N.C. Hsu. 2013. The Collection 6 MODIS aerosol products over land and ocean. *Atmos. Meas. Tech. Discuss., 6,* 159–259, doi:10.5194/amtd-6-159-2013.

Li, C., J.-S. Storch, and J. Marotzke. 2012. Deep-ocean heat uptake and equilibrium climate response. *Clim. Dyn.,* doi:10.1007/s00382-012-1350-z.

Marsland, S.J. and coauthors. 2013. Evaluation of the ocean performance of the ACCESS Climate Model in CMIP5. *Aust. Met. Oceanogr. J., 63,* 101–19.

Martin, G.M., and R.C. Levine. 2012. The influence of dynamic vegetation on the present-day simulation and future projections of the South Asian summer monsoon in the HadGEM2 family. *Earth Sys. Dyn., 3,* 245–261, doi:10.5194/esd-3-245-2012.

Martin, G.M. and coauthors. 2011. The HadGEM2 family of Met Office Unified Model climate configurations. *Geosci. Model Dev., 4,* 723–757, doi:10.5194/gmd-4-723-2011.

Meehl, G.A., C. Covey, B. McAvaney, M. Latif, and R.J. Stouffer. 2005. Overview of the Coupled Model Intercomparison Project. *Bull. Am. Meteorol. Soc., 86,* 89–93, doi:10.1175/BAMS-86-1-89.

Meinshausen, M. and coauthors. 2011a. The RCP greenhouse gas concentrations and their extensions from 1765 to 2300. *Clim. Change, 109,* 213–241, doi:10.1007/s10584-011-0156-z.

Meinshausen, M., S.C.B. Raper, and T.M.L. Wigley. 2011b. Emulating coupled atmosphere-ocean and carbon cycle models with a simpler model, MAGICC6 – Part 1: Model description and calibration. *Atmos. Chem. Phys., 11,* 1417–1456, doi:10.5194/acp-11-1417-2011.

Mitchell, T.D. 2003. Pattern Scaling: An Examination of the Accuracy of the Technique for Describing Future Climates. *Clim. Change, 60,* 217–242, doi:10.1023/A:1026035305597.

Moss, R.H. and coauthors. 2010. The next generation of scenarios for climate change research and assessment. *Nature, 463,* 747–756, doi:10.1038/nature08823.

Myhre, G. and coauthors. 2013. Radiative forcing of the direct aerosol effect from AeroCom Phase II simulations. *Atmos. Chem. Phys., 13,* 1853–1877, doi:10.5194/acp-13-1853-2013.

Nakicenovic, N., and R. Swart, eds. 2000. *IPCC Special Report on Emissions Scenarios*. Cambridge University Press,.

Randall, D.A. and coauthors. 2007. Climate Models and Their Evaluation. *Climate Change 2007: The Physical Science Basis. Contribution of Working Group I to the Fourth Assessment Report of the Intergovernmental Panel on Climate Change*, Eds. S. Olomon, D. Qin, M. Manning, Z. Chen, M. Marquis, K.B. Averyt, M.Tignor, and H.L. Miller, Cambridge University Press.

Rashid, H.A., A.C. Hirst, and M. Dix. 2013. Atmospheric circulations in the ACCESS coupled model: Historical simulations and future projections. *Aust. Met. Oceanogr. J., 63,* 145–60.

Remer, L.A. and coauthors. 2008. Global aerosol climatology from the MODIS satellite sensors. *J. Geophys. Res., 113,* D14S07, doi:10.1029/2007JD009661.

Rogelj, J., M. Meinshausen, and R. Knutti. 2012. Global warming under old and new scenarios using IPCC climate sensitivity range estimates. *Nature Clim. Change, 2,* 248–253, doi:10.1038/nclimate1385.

Sato, M., J.E. Hansen, M.P. McCormick, and J.B. Pollack. 1993. Stratospheric Aerosol Optical Depths, 1850–1990. *J. Geophys. Res., 98,* 22987–22994, doi:10.1029/93JD02553.

Shiogama, H. and coauthors. 2010a. Emission scenario dependencies in climate change assessments of the hydrological cycle. *Clim. Change, 99,* 321–329, doi:10.1007/s10584-009-9765-1.

Shiogama, H., S. Emori, K. Takahashi, T. Nagashima, T. Ogura, T. Nozawa, and T. Takemura. 2010b. Emission Scenario Dependency of Precipitation on Global Warming in the MIROC3.2 Model. *J. Climate, 23,* 2404–2417, doi:10.1175/2009JCLI3428.1.

Smith, R.N.B. 1990. A scheme for predicting layer clouds and their water content in a general circulation model. *Q. J. R. Meteorol. Soc., 116,* 435–460, doi:10.1002/qj.49711649210.

Soden, B.J., A.J. Broccoli, and R.S. Hemler. 2004. On the Use of Cloud Forcing to Estimate Cloud Feedback. *J. Clim., 17,* 3661–3665, doi:10.1175/1520-0442(2004)017<3661:OTUOCF>2.0.CO;2.

Stouffer, R.J. 2004. Time Scales of Climate Response. *J. Clim., 17,* 209–217, doi:10.1175/1520-0442(2004)017<0209:TSOCR>2.0.CO;2.

Taylor, K.E., and C. Doutriaux. 2010. CMIP5 Model Output Requirements: File Contents and Format, Data Structure and Metadata. 37 pp. http://cmip-pcmdi.llnl.gov/cmip5/docs/CMIP_output_metadata_requirements.pdf.

Taylor, K.E., R.J. Stouffer, and G.A. Meehl. 2009. A Summary of the CMIP5 Experiment Design. PCDMI Rep., 33 pp. [Available online at http://cmip-pcmdi.llnl.gov/cmip5/docs/Taylor_CMIP5_design.pdf.]

Taylor, K.E., V. Balaji, S. Hankin, M. Juckes, B. Lawrence, and S. Pascoe. 2011. CMIP5 Data Reference Syntax (DRS) and Controlled Vocabularies. 14 pp. http://cmip-pcmdi.llnl.gov/cmip5/docs/cmip5_data_reference_syntax.pdf.

Taylor, K.E., R.J. Stouffer, and G.A. Meehl. 2012. An Overview of CMIP5 and the Experiment Design. *Bull. Am. Meteorol. Soc., 93,* 485–498, doi:10.1175/BAMS-D-11-00094.1.

Textor, C. and coauthors. 2006. Analysis and quantification of the diversities of aerosol life cycles within AeroCom. *Atmos. Chem. Phys., 6,* 1777–1813, doi:10.5194/acp-6-1777-2006.

Uotila, P., S. O'Farrell, S.J. Marsland, and D. Bi. 2013. The sea-ice performance of the Australian models participating in the CMIP5. *Aust. Met. Oceanogr. J., 63,* 121–43.

Vecchi, G.A., and B.J. Soden. 2007. Global Warming and the Weakening of the Tropical Circulation. *J. Clim., 20,* 4316–4340, doi:10.1175/JCLI4258.1.

Van Vuuren, D.P. and coauthors. 2011. The representative concentration pathways: an overview. *Clim. Change, 109,* 5–31, doi:10.1007/s10584-011-0148-z.

Wang, Y.-M., J.L. Lean, and N.R. Sheeley, Jr. 2005. Modeling the Sun's Magnetic Field and Irradiance since 1713. *Astrophys. J., 625,* 522–538, doi:10.1086/429689.

Watanabe, S. and coauthors. 2011. MIROC-ESM 2010: model description and basic results of CMIP5-20c3m experiments. *Geosci. Model Dev., 4,* 845–872, doi:10.5194/gmd-4-845-2011.

Watterson, I.G. 2011. Understanding and partitioning future climates for Australian regions from CMIP3 using ocean warming indices. *Clim. Change, 111,* 903–922, doi:10.1007/s10584-011-0166-x.

Watterson, I.G., and P.H. Whetton. 2011. Distributions of decadal means of temperature and precipitation change under global warming. *J. Geophys. Res., 116,* doi:10.1029/2010JD014502.

Williams, D.N. and coauthors. 2009. The Earth System Grid: Enabling Access to Multimodel Climate Simulation Data. *Bull. Am. Meteorol. Soc., 90,* 195–205, doi:10.1175/2008BAMS2459.1.

Wilson, D.R., A.C. Bushell, A.M. Kerr-Munslow, J.D. Price, and C.J. Morcrette. 2008. PC2: A prognostic cloud fraction and condensation scheme. I: Scheme description. *Q. J. R. Meteorol. Soc., 134,* 2093–2107, doi:10.1002/qj.333.

Winton, M., K. Takahashi, and I.M. Held. 2010. Importance of Ocean Heat Uptake Efficacy to Transient Climate Change. *J. Clim., 23,* 2333–2344, doi:10.1175/2009JCLI3139.1.

Woodward, S. 2001. Modeling the atmospheric life cycle and radiative impact of mineral dust in the Hadley Centre climate model. *J. Geophys. Res., 106,* 18155–18166, doi:10.1029/2000JD900795.

Woodward, S. 2011. *Mineral Dust in HadGEM2*. Hadley Centre Tech. Note 87.

Yu, F., G. Luo, and X. Ma. 2012. Regional and global modeling of aerosol optical properties with a size, composition, and mixing state resolved particle microphysics model. *Atmos. Chem. Phys., 12,* 5719–5736, doi:10.5194/acp-12-5719-2012.

Yue, X., and H. Liao. 2012. Climatic responses to the shortwave and longwave direct radiative effects of sea salt aerosol in present day and the last glacial maximum. *Clim. Dyn., 39,* 3019–3040, doi:10.1007/s00382-012-1312-5.

Zender, C.S., R.L. Miller, and I. Tegen. 2004. Quantifying mineral dust mass budgets: Terminology, constraints, and current estimates. *EOS Trans. Am. Geophys. Union, 85,* 509, doi:10.1029/2004EO480002.